

Ab-initio study of different structures of CaC ionic compound: Magnetism, Bonding, Exchange interaction and Lattice Dynamics

Zahra Nourbakhsh, S. Javad Hashemifar,* and Hadi Akbarzadeh
Department of Physics, Isfahan University of Technology, 84156-83111 Isfahan, Iran

On the basis of density functional - pseudopotential calculations, we study structural, electronic, magnetic, and mechanical properties of the hypothetical CaC ionic compound in the rock-salt (RS), B2, zinc-blende (ZB), wurtzite (WZ), NiAs (NA), and anti-NiAs (NA*) structures. The results show that RS-CaC is the most stable system at equilibrium while applying negative hydrostatic pressures may stabilize the half-metallic WZ and ZB structures. The ferromagnetic equilibrium state observed in the RS, ZB, NA and WZ structures of CaC is attributed to the sharp partially filled \mathbf{p} band of the carbon atom. It is argued that the ionic interaction increases the sharpness of the \mathbf{p} band and hence enhances ferromagnetism while the covalent interaction increases the band dispersion and weakens magnetism. We investigate various properties of the exchange interaction in the ferromagnetic CaC structures. It is observed that the interatomic exchange interaction in these systems have consistent behavior with the spin splittings of the bond points. Comparing the structural properties in the ferromagnetic and nonmagnetic states, indicates a weak magneto-structural coupling in CaC. Applying non-local corrections to the exchange functional enhance the exchange splitting and hence give rise to a half-metallic electronic structure for the WZ, RS, and NA structures of CaC. In the framework of density functional perturbation theory, the phonon spectra of these systems are investigated and the observed dynamical instabilities in the NA* and B2 structures are attributed to the tendency of the carbon atoms toward dimerization. Various mechanical properties of the dynamically stable structures of CaC are determined from their phonon spectra.

I. INTRODUCTION

Recent observation of \mathbf{p} magnetism in some materials has attracted considerable research interest as a novel magnetic phenomenon different from conventional magnetic phenomena originating from a partially filled \mathbf{d} or \mathbf{f} shell.¹ Using first-principle calculations, in 2004, Kusakabe *et al.*² predicted a new class of the \mathbf{p} magnetic systems in some hypothetical binary ionic compounds with no transition metals including CaP, CaAs and CaSb. The additional advantage of these systems is that in the metastable zinc-blende (ZB) phase, these compounds show half-metallic behavior which is attractive in the Spintronics community.³ In a half-metal, only one spin channel contributes to the states around the Fermi level.

Later on, Sieberer *et al.*,⁴ predicted half-metallicity in the hypothetical ZB structure of several other $\text{II}^A\text{-V}^A$, $\text{II}^A\text{-IV}^A$, and $\text{I}^A\text{-V}^A$ compounds such as CaN, CaC, and LiP. In all of these ionic binary compounds, the partially occupied sharp \mathbf{p} band of the anion atom enhances the Stoner exchange interaction and thus give rises to a ferromagnetic (FM) ground state. This mechanism is schematically sketched in Fig. 1. As it is qualitatively argued in the figure, if exchange splitting is larger than band width, a half-metallic gap appears in the majority channel. The flatness of the \mathbf{p} band is controlled by the cell volume, system ionicity, and slight \mathbf{p} - \mathbf{d} hybridization around the Fermi level.⁴

Two major open issues in the novel \mathbf{p} magnetic compounds are their stable structure and properties of the exchange interaction in these systems. First-principles investigations may provide very helpful and accurate information for understanding these open issues. A point worth to mention is that in conventional ferromagnets,

as the highly correlated \mathbf{d} or \mathbf{f} electrons have the key role, more accurate many body calculations are usually needed to describe the system while in the \mathbf{p} magnets less expensive exchange-correlation calculations are expected to be sufficient.

In this paper, we focus on the hypothetical CaC compound as a potential \mathbf{p} magnetic system and apply density functional calculations to investigate its structural and magnetic properties in six different structures: cubic rock-salt (RS), cesium chloride (B2) and ZB and hexagonal wurtzite (WZ), NiAs (NA) and anti-NiAs (NA*) structures. The NA* structure is made by permuting Ni and As in the NA structure. The natural compound of Ca and C is CaC_2 that is a nonmagnetic insulator and crystallizes in the rock-salt structure in which C_2^{2-} dimers and Ca^{2+} ions occupy the 4a and 4b wyckoff positions.⁵ Understanding the \mathbf{p} ferromagnetism in the hypothetical CaC compound may provide new opportunities for developing ferromagnetic carbon nanostructures.

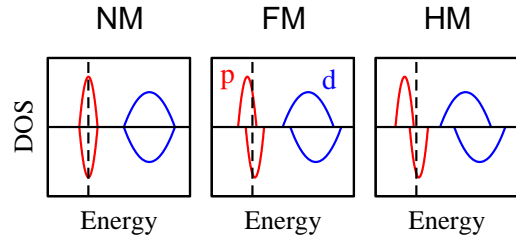


FIG. 1: (Color online) Schematic spin resolved density of states (DOS) of a \mathbf{p} magnetic system in the non-magnetic (NM), ferromagnetic (FM) and half-metallic (HM) states. The upward and downward plots show the majority and minority states and the dashed lines show the Fermi energy.

TABLE I: Reciprocal space grids applied to the PBE, phonon and HSE calculations.

	PBE	Phonon	HSE
RS	$10 \times 10 \times 10$	$4 \times 4 \times 4$	$5 \times 5 \times 5$
ZB	$10 \times 10 \times 10$	$4 \times 4 \times 4$	$5 \times 5 \times 5$
WZ	$12 \times 12 \times 10$	$5 \times 5 \times 4$	$5 \times 5 \times 5$
NA	$15 \times 15 \times 9$	$5 \times 5 \times 3$	$5 \times 5 \times 3$
B2	$20 \times 20 \times 20$	$6 \times 6 \times 6$	—
NA*	$16 \times 16 \times 16$	$5 \times 5 \times 5$	—

After reviewing our computational methods in the next section, the structural and magnetic properties of all selected CaC structures will be discussed in section III. Then various properties of the exchange interaction in CaC compound will be analyzed in section IV. Next, the phonon spectra of the systems will be presented to investigate the dynamical stability and elastic properties of the CaC structures. Our conclusions are presented in the last section.

II. COMPUTATIONAL METHODS

The geometry optimizations and electronic structure calculations are carried out by using the PWscf code of the QUANTUM-ESPRESSO package.⁶ The generalized gradient approximation (GGA) in the scheme of Perdew, Burke and Ernzerhof (PBE)⁷ and norm-conserving pseudopotentials,⁸ by considering 10 valence electrons for Ca and 4 valence electrons for C, were used throughout our calculations. The Kohn-Sham single particle wave functions were expanded in plane wave basis set up to energy cutoff of 80 Ry and the Fourier expansion of electron density were cut at 320 Ry.

The Brillouin zone integrations were performed on the Γ -centered symmetry-reduced Monkhorst-Pack⁹ k-point meshes (table I), using the Methfessel-Paxton¹⁰ smearing method with a broadening parameter of 1 mRy. All computational parameters were optimized to achieve total energy accuracy of about 0.1 mRy/formula unit (*fu*). The electronic structure calculations were performed in the scalar relativistic limit, ignoring the relativistic spin-orbit interaction which is expected to be small in the light carbon and calcium atoms. The phonon frequencies are calculated using the density functional linear response method for metallic systems.¹¹ Table I lists the reciprocal space grids used for the expensive phonon calculations.

We employ topological analysis of the total as well as spin resolved electron charge density,¹² for accurate description of bonding and magnetism in the systems. In this scheme, bond points are defined as the saddle points of electron density between neighboring nuclei. At the bond saddle points, electron density displays a minimum in the bond direction and two maxima in the perpendicular directions.

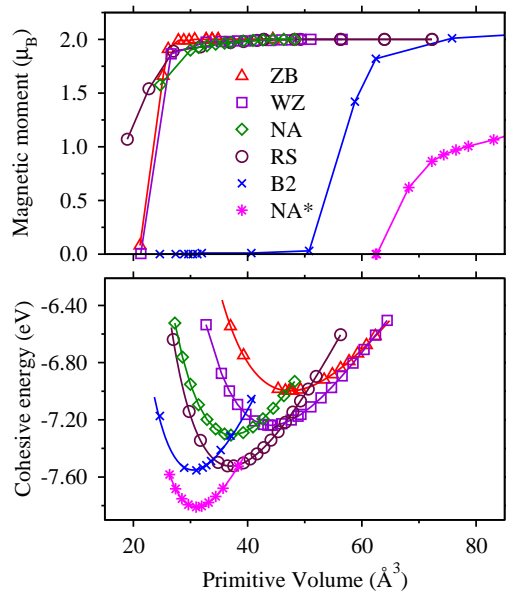


FIG. 2: (Color online) Calculated cohesive energy and magnetic moment (per formula unit) of CaC in the six studied structures as a function of the primitive volume. The total energy diagrams are plotted in limited ranges around the equilibrium volumes while a broader range is used for plotting the diagrams of the magnetic moments.

III. STRUCTURAL AND MAGNETIC PROPERTIES

In order to find the structural properties of CaC in the selected structures, we computed the primitive cell energy of all structures as a function of the primitive volume, in the ferromagnetic and nonmagnetic phases. The B2 and NA* structures of CaC were found to be nonmagnetic around the equilibrium volume, while other systems (ZB, WZ, NA, and RS) stabilized in a ferromagnetic ground state. The total energy and magnetic moment of all systems in their stable magnetic states are plotted as a function of volume in Fig. 2. It is observed that the nonmagnetic NA* and B2 structures have the lowest energies, while the ferromagnetic ZB phase is the highest energy metastable structure among the studied systems. The equilibrium magnetic moments of WZ, RS, and NA ferromagnetic structures are slightly less than $2 \mu_B/fu$ while the ferromagnetic ZB-CaC has an integer moment of $2 \mu_B/fu$. The integer value of the total magnetic moment in the ZB structure evidences the half-metallic behavior of this high energy metastable structure, while other ferromagnetic structures require some negative pressures (volume expansion) to achieve a half-metallic electronic structure.

In order to address the relative stability of the studied systems at elevated pressures, we calculated and plotted in Fig. 3, the enthalpy free energy (H) of the systems: $H = E - pV$, where E is the converged primitive cell energy, V is the primitive volume, and p is the hydrostatic

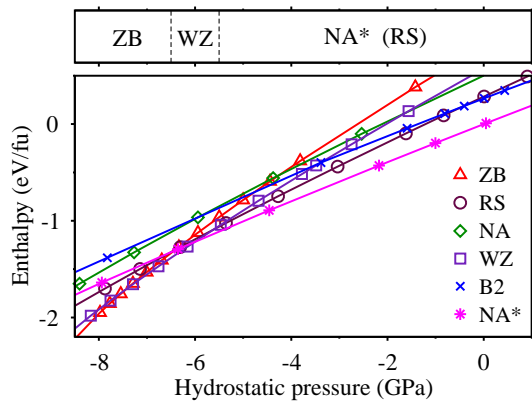


FIG. 3: (Color online) Calculated enthalpy free energy of CaC in the six studied structures as a function of the hydrostatic pressure and the resulting pressure phase diagram.

pressure calculated from the slope of the energy-volume curves. The resulting simple pressure phase diagram, plotted in the same figure, indicates thermodynamic stability of the NA* structure at the pressures above about -5.5 GPa and RS is the second stable structure in this region. Because of the dynamical instability of the NA* and B2 structures, will be shown in the section "Dynamical properties", in practice, the RS structure is expected to be the most stable phase at the pressures above -5.5 GPa. Below this transition pressure, the WZ structure becomes more stable. The pressure induced RS-WZ structural transition seems to be a first order transition, because the enthalpy of these two structures does not connect smoothly at the transition pressure. Inspecting the calculated magnetic moments (Fig. 2) indicates that the RS-WZ structural transition is accompanied by a normal ferromagnet to half-metal phase transition. The ZB structure finds thermodynamic stability after a further transition at a pressure of about -6.5 GPa. Although, the obtained phase diagram shows the stability of the half-metallic systems in the negative pressures, advanced epitaxial growth techniques make it feasible to synthesize the stretched thin films of these systems on proper substrates.

The calculated equilibrium properties determined by fitting the Murnaghan equation of state¹³ to the calculated total energy-volume data are presented in Fig. 4. It is seen that in the sequence of ZB, WZ, NA, RS, B2, and NA* structures, the cohesive energy, equilibrium volume, and compressibility (inverse of the bulk modulus) are decreasing. These behaviors indicate enhancement of the bond strength and bond stiffness in this sequence. For better understanding, the ionization parameter I and the total electron density at bond points ρ_B (per formula unit) are also computed and plotted in Fig. 4. The ionization parameter, defined as the transferred charge from cation to anion normalized by the cation valence charge, is a measure of the ionic interaction in the systems. On the other hand, ρ_B is the sum of electron densities at

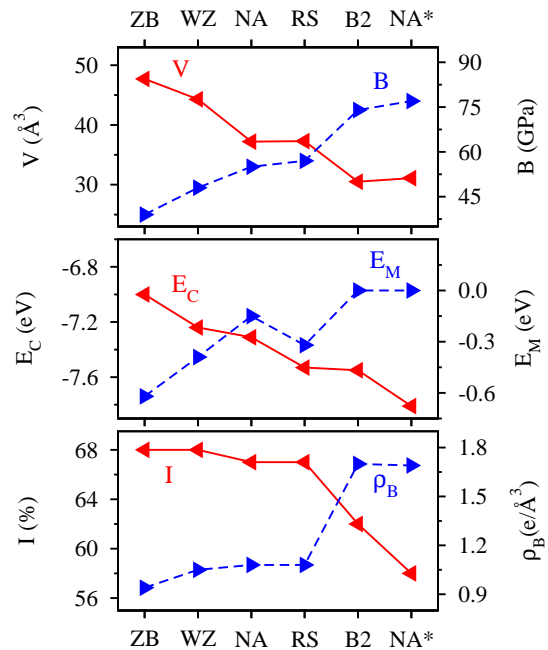


FIG. 4: (Color online) Calculated equilibrium properties of CaC in the selected structures. V : equilibrium primitive volumes, B : bulk modulus, E_C : cohesive energy, E_M : magnetization energy defined as the difference between the ferromagnetic and nonmagnetic cohesive energies, I : ionization, ρ_B : total electron density at bond points.

all topological bond points (per formula unit) and thus speculates the strength of the covalent bonding in the systems. We observe that the enhancement of the bond strength and stiffness in the studied systems is accompanied by decreasing the ionic and increasing the covalent interactions in the systems. It is known that the directional covalent bonds form solids with high strength, high stiffness, and high melting point while ionic interaction typically give rises to intermediate strength and extremely brittle solids. In the next sections, we qualitatively compare the brittleness of the systems. The calculated results (Fig. 4) indicate that the nonmagnetic B2 and NA* structures exhibit the highest covalency and the lowest ionization among the studied systems. Moreover, we observe that the more ionized structures (except NA) have larger absolute magnetization energies. These observations are evidences for the ionic origin of ferromagnetism in CaC.

The equilibrium lattice parameters, Fermi level spin polarizations, bond lengths, and atomic magnetic moments in the six studied lattices of CaC are listed in table II. After topological analysis of charge densities, we identified that, in addition to the ionic carbon-calcium bonding in all systems, there are some covalent carbon-carbon bonds in the nonmagnetic NA* and B2 structures. Therefore, equilibrium properties of the C-C bond, in addition to C-Ca, are also listed in table II. In order to understand these results, we note that while the C-Ca interaction is mainly ionic, the C-C bonding is totally cova-

TABLE II: Computed equilibrium lattice parameters a and c , atomic and total magnetic moments, and C-C and C-Ca bond properties in the selected structures of CaC; $P(\%)$: total spin polarization at the Fermi level, $d(\text{\AA})$: equilibrium distance, N_b : number of the topological bonds per formula unit, and ρ_b ($e/\text{\AA}^3$): bond electron density. The WZ structure involves slightly different vertical and in-plane bonds and hence, in this case, the average bond properties are reported.

	a	c	P	magnetic moments			C – C			C – Ca		
				C	Ca	total	d	N_b	ρ_b	d	N_b	ρ_b
NA*	4.19	4.06	0	0	0	0.00	2.03	1	0.49	2.62	6	0.20
B2	3.13	—	0	0	0	0.00	3.13	3	0.14	2.71	8	0.16
RS	5.29	—	70	1.78	0.21	1.97	3.74	0	—	2.65	6	0.18
NA	3.64	6.48	70	1.80	0.19	1.98	3.64	0	—	2.65	6	0.18
WZ	4.38	5.30	90	1.81	0.21	1.99	3.66	0	—	2.58	5	0.20
ZB	5.75	—	100	1.86	0.19	2.00	4.07	0	—	2.49	4	0.24

lent. Observation of the topological covalent C-C bonds in the nonmagnetic B2 and NA* structures explains the highest covalency of these systems (Fig. 4). Moreover, the slight increasing of the magnetic moment in RS, NA, WZ, and ZB series is generally accompanied by increasing (decreasing) the C-C (C-Ca) distance. Decreasing the C-Ca distance intensifies the ionic attraction in the systems and hence enhances the magnetic moment via increasing the charge transferred from Ca to the flat C p orbital (Fig. 4). In contrary, the reduction of the C-C distance enhances the covalent interaction in the system and consequently increases the valence band width and then decreases the magnetic moment. These findings, further evidence that ferromagnetic behavior of CaC roots into the ionic C-Ca interaction.

All magnetic structures show a magnetic moment of about $2 \mu_B/fu$ with no topological covalent C-C bond. In the ZB structure, the magnetic moment is exactly equal to $2 \mu_B/fu$ which is due to the half-metallic behavior of this system argued by the calculated perfect Fermi level spin polarization (table II). We observe that the magnetic moments are mainly carried by the C atoms and the Ca atoms have a small moment parallel to the C moment. The dominant magnetic contribution of carbon comes from the strong ionic C-Ca interaction which highly evacuates the valence s shell of calcium. The empty spin down C p orbital give rises to more charge transferring in the minority channel and leaving a positive moment on the Ca atom. All FM structures of CaC have a perfect or nearly semiconducting majority channel and the Fermi level spin polarizations comes form the minority electrons. Hence it seems that these systems are capable of conducting spin currents antiparallel to their magnetic moment.

It was mentioned that all systems have C-Ca bonds while the topological C-C bonds appear only in the non-magnetic NA* and B2 structures (table II). In the NA* structure, strong covalent bonding between C atoms significantly decrease the c/a ratio while in the NA lattice the mainly ionic C-Ca interaction increases this ratio. A visible trend is that systems with higher number of bonds per atom (N_b) have generally smaller electron densities

at bond points (ρ_b) and longer bond lengths. It may be explained in this way that in these systems the valence electrons are divided into more bonds, hence each bond receives less electrons and consequently gets weaker and longer. However, overall bonding in the highly coordinated systems is stronger, because these systems have generally lower cohesive energy and higher total electron density at bond points (Fig. 4).

The heat of formation (ΔH_f) of bulk CaC which measures the required energy to decompose this compound into graphite and bulk fcc Ca, is calculated as follows:

$$\Delta H_f = E_{coh}^{CaC} - (E_{coh}^C + E_{coh}^{Ca})$$

where the right hand side parameters are the cohesive energies of bulk CaC, graphite, and bulk fcc calcium. The calculated formation energies of CaC in the studied structures are 1.83 eV (NA*), 2.1 eV (B2), 2.1 eV (RS), 2.3 eV (NA), 2.4 eV (WZ) and 2.6 eV (ZB). These positive formation energies indicate that synthesis of these systems requires endothermic processes.

IV. EXCHANGE INTERACTION IN CaC

As it was mentioned, an important issue in the novel field of p magnetism, is understanding the properties of the exchange interaction in these systems. In this regard, we investigate various spin dependent parameters in CaC ferromagnetic structures (ZB, WZ, RS, NA) to discuss some features of the exchange interaction in this system.

A. Exchange stiffness

The first calculated parameter is the energy difference between the ferromagnetic and antiferromagnetic (AF) spin states of CaC in the selected structures. Applying a simple effective Heisenberg model to the exchange interaction between the nearest neighbor carbon atoms with magnetic moments M_1 and M_2 : $E = J/2(M_1 \cdot M_2)$ enables us to estimate the interatomic exchange stiffness

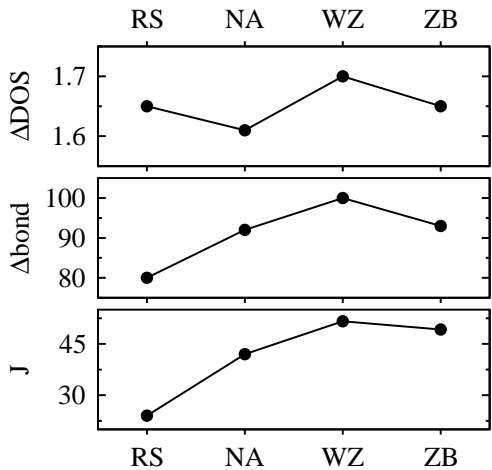


FIG. 5: Calculated exchange stiffness J (meV), bond spin splitting Δbond (mÅ), and exchange splitting of the carbon \mathbf{p} states ΔDOS (eV) in the ferromagnetic CaC structures.

from the energy difference of the FM and AF states: $J = (E_{AF} - E_{FM})/|M|^2$. The estimated J parameters may be used for qualitative comparison of the Curie temperatures of different systems. In the hexagonal NA and WZ structures, the AF spin ordering were applied in the [0001] direction while in the cubic RS and ZB structures we calculated and compared the minimized energy of the type I (AF ordering in the [001] direction) and type II (AF ordering in the [111] direction) antiferromagnetism and found that both structures prefer AF-type II. Employing the obtained antiferromagnetic energies, the interatomic exchange stiffness between the nearest C atoms in the different CaC structures was estimated to be about 24 meV (RS), 42 meV (NA), 52 meV (WZ), and 49 meV (ZB). Hence, it is speculated that WZ and ZB have the highest Curie temperatures among these four structures. The obtained J values, plotted in Fig. 5, are substantially larger than the exchange stiffness of some strong ferromagnets such as Co_2MnSi Heusler alloy.¹⁴ Then, RS-, WZ-, ZB-, and NA-CaC are expected to be high Curie temperature ferromagnets and thus promising for practical applications. The theoretical Curie temperature of ZB-CaC, in the mean field and random phase approximations, is reported to be about 1051 and 735 K, respectively.¹⁵

B. Exchange splittings

The spin resolved partial electronic density of states (DOS) of the valence states of CaC in its ferromagnetic structures are displayed in Fig. 6. It is seen that the carbon \mathbf{p} states have the dominant contribution to the valence band with slight hybridization with the calcium \mathbf{d} states. Therefore, magnetization mainly comes from the carbon \mathbf{p} electrons (Table. II). The valence bands in the ZB structure are considerably sharper, compared with

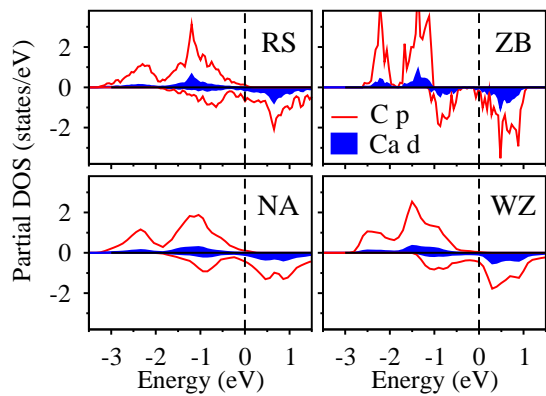


FIG. 6: (Color online) Calculated partial DOS of the carbon \mathbf{p} (solid line) and calcium \mathbf{d} (shaded areas) orbitals in the ferromagnetic CaC structures. The positive and negative densities correspond to the majority and minority states, respectively. The Fermi energies are set to zero.

the other three structures. This observation explains the half-metallic behavior of ZB-CaC in equilibrium volume. By using the sharp peaks of the partial DOS in the majority and minority channels, we estimated the exchange splitting of the carbon \mathbf{p} states in all ferromagnetic structures and plotted the obtained data in Fig. 5. It is clearly visible that the exchange splitting of the partial \mathbf{p} DOS is not correlated with the exchange stiffness parameter. The reason is that the interatomic exchange coupling constant J only measures the exchange interaction between the neighboring carbon valence electrons while the exchange splitting of the carbon \mathbf{p} states originates from the full exchange interaction between all valence states. In other words, the on-site exchange interaction plays an important role in the exchange splitting of the carbon \mathbf{p} states while it has small effect on the interatomic exchange coupling. An evidence for this fact is that, when the interatomic distances increase to large values, the on-site exchange splittings are usually enhanced while the interatomic exchange couplings vanish.

Since the bond points are rather far from the nuclei, their spin dependent properties are expected to be less sensitive to the on-site exchange interaction and thus better correlated with the interatomic exchange coupling. In order to verify this statement, we applied topological analysis to the spin resolved electron densities to find the majority and minority bond positions in the ferromagnetic structures. The distance between the spin resolved topological bond points is defined as the bond spin splitting and plotted in Fig. 5. As it was stated, we observe a clear correlation between this distance and the exchange stiffness. Therefore, the bond spin splitting may be assumed as the real space representation of the interatomic exchange interaction in ferromagnetic materials.

TABLE III: Calculated cohesive energy (E_C), equilibrium volume (V_0), bulk modulus (B), ionization (I), and bond electron density (ρ_b) of the ferromagnetic structures of CaC and the ZB structure of MnAs and CrAs in the nonmagnetic (NM) and ferromagnetic (FM) phases.

	Lattice	E_C (eV)		V_0 (\AA^3)		B (GPa)		I (%)		ρ_b ($e/\text{\AA}^3$)	
		FM	NM	FM	NM	FM	NM	FM	NM	FM	NM
CaC	RS	-7.53	-7.21	37.1	36.0	60	60	67	65	0.18	0.18
	NA	-7.31	-7.16	37.2	35.2	57	65	67	66	0.18	0.19
	WZ	-7.24	-6.85	44.1	44.3	48	47	68	68	0.20	0.20
	ZB	-7.00	-6.38	47.5	46.5	42	41	68	68	0.24	0.25
MnAs	ZB	-6.28	-5.39	46.1	37.3	50	105	—	—	0.43	0.59
CrAs	ZB	-6.35	-5.30	45.3	39.7	67	96	—	—	0.46	0.55

C. Magneto-structural coupling

In order to study the interplay between magnetism and bonding, we calculated the structural properties of the ferromagnetic structures of CaC in the nonmagnetic state. The results, presented in table III, point to an interesting property of this class of magnetic materials; the equilibrium volume and bulk modulus are nearly independent of the magnetic state. It is then concluded that the exchange interaction in the CaC structures weakly affects the structural parameters of the system. For more understanding, we calculated the equilibrium volume and bulk modulus of ZB-MnAs and ZB-CrAs in the ferromagnetic and nonmagnetic states (table III) and observed that the nonmagnetic systems have considerably higher bulk modulus and lower equilibrium volume. Since magnetism in MnAs and CrAs originates from the partially filled $3d$ states, it is concluded that the interplay between bonding and magnetism in the \mathbf{p} magnetic systems, in contrast to the \mathbf{d} magnetic systems, is weak.

For understanding the magneto-structural coupling, one should take into account the way the exchange interaction influences the spatial distribution of electrons in a magnetic system. The exchange interaction, in general, transfers some electrons from the occupied minority states into the unoccupied majority states. Because of the symmetry splitting of the \mathbf{d} orbital in all crystal structures, the occupied and unoccupied \mathbf{d} valence states have always different orbital character and spatial distribution. For example, in the cubic crystal field, the \mathbf{d} orbital splits into the triply degenerate \mathbf{t}_2 and the doubly degenerate \mathbf{e} states with different spatial distribution. Among these two sub-orbitals, the one that contributes more in the interatomic bonds has lower energy and hence is more occupied while the higher energy and less occupied sub-orbital distributes in the out-of-bond regions of the lattice. Therefore, the exchange induced charge transfer in the \mathbf{d} magnetic systems usually weakens the bonds by driving the minority electrons of the interatomic bonds toward the out-of-bond regions of the lattice where the majority unoccupied states are distributed. As a result of that, the exchange interaction

in these systems acts as an effective repulsive force and hence increases the interatomic distances and compressibility of the systems.

On the other hand, the \mathbf{p} orbital is less influenced by the crystal symmetries. We focus on the cubic symmetry, in which the spin resolved \mathbf{p} orbitals are triply degenerate and hence the occupied and unoccupied \mathbf{p} valence states have similar spatial distributions. As a result of that, in the cubic \mathbf{p} magnetic systems, the exchange induced charge transfer preserves the spatial distribution of electrons and consequently the nonmagnetic and magnetic phases of these systems have close interatomic distances and compressibilities. In other words, the exchange interaction in the \mathbf{p} magnetic materials, mainly influences the local spin distribution of electrons without significant effect on the total electron density. In order to verify this statement, we calculated the ionization and bond electron density of RS-, NA-, WZ-, and ZB-CaC as well as ZB-MnAs and ZB-CrAs in the nonmagnetic and ferromagnetic states (table III). It is clearly seen that in the CaC structures, nonmagnetic and ferromagnetic systems, have very similar ionizations and bond electron densities, while in the \mathbf{d} ferromagnet CrAs and MnAs, the exchange interaction effectively reduces the bond electron densities of the ferromagnetic states, compared with the nonmagnetic states.

The splitting of the \mathbf{p} orbital into \mathbf{p}_z and \mathbf{p}_{xy} , in the hexagonal symmetry, may enhance magneto-structural coupling in the hexagonal \mathbf{p} magnetic systems. In the hexagonal NA-CaC, \mathbf{p}_z has lower energy and more contribution to bonding. Hence, the exchange interaction transfers some minority \mathbf{p}_z electrons into the empty majority \mathbf{p}_{xy} states and consequently enhances bonding in the xy plane. As a result of that, NA-CaC in the ferromagnetic state, compared with the nonmagnetic state, has smaller in-plane and larger vertical lattice parameter, giving rise to a slightly larger equilibrium volume and compressibility for the ferromagnetic state. On the other hand, in the hexagonal WZ-CaC, the exchange induced in-plane bond enhancement and vertical bond weakening compensate each other and hence the FM and NM phases of this system have close equilibrium volume and bulk modulus.

TABLE IV: Calculated equilibrium volume (V_0), bulk modulus (B), cohesive energy (E_C), magnetic moment (μ), spin flip gap ($sgap$), and exchange splitting of DOS (ΔDOS) in ferromagnetic structures of CaC within the HSE03 and PBE functionals.

	V_0 (\AA^3)		B (GPa)		E_C (eV)		μ (μ_B)		$sgap$ (eV)		ΔDOS (eV)	
	HSE	PBE	HSE	PBE	HSE	PBE	HSE	PBE	HSE	PBE	HSE	PBE
RS	37.2	37.1	62	60	-7.06	-7.53	2.00	1.97	0.8	0	3.35	1.65
NA	37.2	37.2	59	57	-6.84	-7.31	2.00	1.98	0.8	0	2.90	1.61
WZ	44.1	44.1	49	48	-6.78	-7.24	2.00	1.99	0.8	0	3.00	1.70
ZB	47.6	47.5	42	42	-6.51	-7.00	2.00	2.00	1.8	0.9	2.95	1.65

D. Non-local exchange effects

The localized nature of the conventional exchange-correlation functionals give rises to the typical underestimation of the semiconductor band gaps, compared with the experimental data.¹⁶ Therefore, because of the semiconducting behavior of half-metals in one spin channel, the non-local exchange effects may significantly influence the half-metallic properties. The calculated Fermi level spin polarizations (table II) and density of states (Fig. 6) within the localized PBE functional, indicate half-metallic behavior of ZB-CaC at its equilibrium volume and nearly half-metallic character of the other ferromagnetic structures of CaC. Thus applying a more accurate non-local exchange-correlation functional may significantly improve the observed half-metallic and nearly half-metallic properties.

We use the screened HSE03 hybrid functional to apply the non-local exchange corrections to our calculations.¹⁷ In this scheme the short range (SR) part of the Hartree-Fock exchange is mixed with the short range PBE exchange while the long range (LR) part of the exchange and whole correlation is taken from the PBE functional:

$$E_{xc}^{HSE} = \frac{1}{4}E_x^{HF,SR} + \frac{3}{4}E_x^{PBE,SR} + E_x^{PBE,LR} + E_c^{PBE}$$

The exclusion of the long range Hartree-Fock exchange from the screened HSE03 hybrid functional efficiently improves its performance in metallic systems. Moreover, this feature substantially reduces the required reciprocal space grids for performing the expensive non-local HSE calculations (table I).

The calculated structural and magnetic properties of CaC in its four ferromagnetic structures within the HSE hybrid functional are presented in table IV along with the corresponding PBE results for comparison. The parameter *spin flip gap* in a half-metal denotes the energy distance between the valence band maximum in the semiconducting spin channel and the Fermi level and hence measures the minimum energy required to flip spin of an electron in the semiconducting spin channel. This parameter may be used to qualify half-metals, because if it vanishes, the half-metallicity breaks. As it was expected, we observe that the non-local exchange effects efficiently improve spin flip gap and exchange splitting of DOS and hence give rises to the half-metallic behavior of all CaC

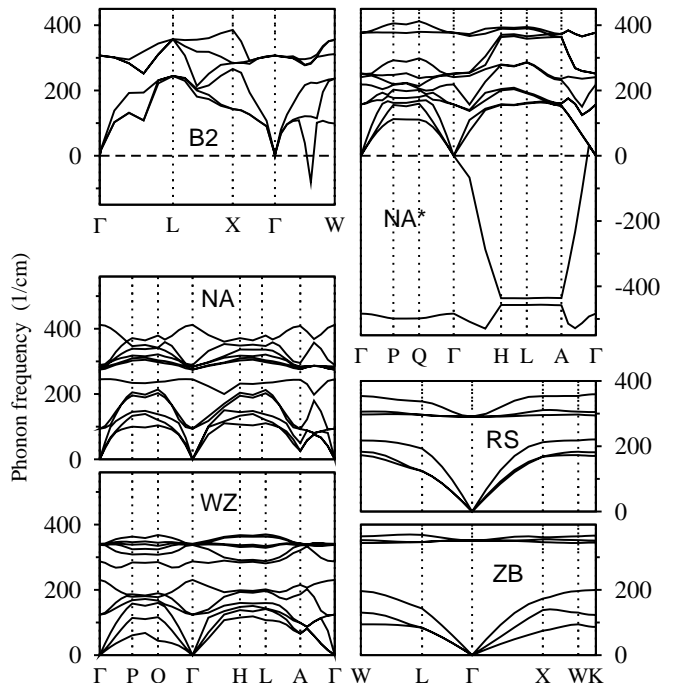


FIG. 7: Calculated phonon band structure of CaC in the B2, RS, ZB, NA*, NA, and WZ structures. The bands are plotted in comparable scales.

ferromagnetic structures within HSE.

Comparing the calculated equilibrium volumes and bulk moduli within the HSE and PBE functionals provides further evidence for the weakness of the magneto-structural coupling in the \mathbf{p} magnetic systems. It is clearly seen that the non-local exchange interactions, in spite of the significant influence on the magnetic parameters, have negligible effect on the equilibrium volumes and bulk moduli. The HSE cohesive energies are found to be about 0.4 eV higher than the PBE values (table IV). It may be attributed to the absence of the self interaction in the Hartree-Fock exchange energy.

V. DYNAMICAL PROPERTIES

The dynamical properties of CaC in the cubic RS, ZB, and B2 and hexagonal WZ, NA, and NA* structures are

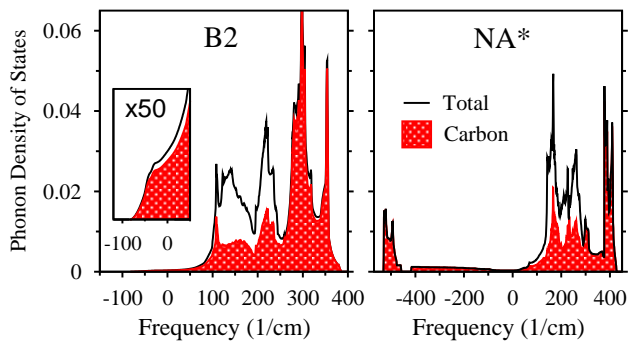


FIG. 8: (Color online) Total phonon DOS (solid line) and carbon contribution to the phonon DOS (shaded area) in the B2 and NA* structures of CaC. The phonon DOS of the B2 structure in the negative (imaginary) frequencies is enlarged 50 times (inset) to be more visible.

studied by calculating the phonon spectra of these systems in the framework of density functional perturbations theory.¹¹ The obtained phonon band structures in the equilibrium ground states are displayed in Fig. 7. The negative values in these plots correspond to the imaginary phonon frequencies. It is observed that the B2 and NA* structures which are the lowest energy systems among the studied structures, have some imaginary phonon frequencies and hence are dynamically unstable. The dynamical instability of the B2 structure occurs in some transverse acoustic phonon modes in a small portion of the BZ in the [110] direction while NA*-CaC has a broad instability coming from an optical phonon band in the whole BZ and a longitudinal acoustic band in the [0001] direction.

In order to understand the origin of the dynamical instabilities, we calculated the atom resolved phonon density of states of the B2 and NA* structures (Fig. 8). It is clearly seen that the imaginary phonon frequencies mainly come from carbon oscillations. This observation indicates that the dynamical instability of the B2 and NA* structures is due to the tendency of the carbon atoms for reconfiguration. Existence of the carbon dimers in the natural CaC₂ compound,⁵ provides an experimental evidence for the tendency of carbons in CaC to get close together and dimerize. This statement, is verified by the topological investigation of the electron density of the B2 and NA* structures. The results, partially displayed in Fig. 9, indicates formation of the topological bonds between the carbon atoms in these two structures. As it is visible in the figure, in the B2 structure, the coplanar covalent carbon-carbon bonds may give rise to reconfiguration (dimerization) of the carbon atoms in the diagonal [110] (and other equivalent) directions. It is consistent with the observed dynamical instability of B2-CaC in the [110] ΓW direction (Fig. 7). Similar arguments apply to the phonon instabilities of NA*-CaC.

The phonon spectra of materials is a rich source of information on mechanical and thermodynamical prop-

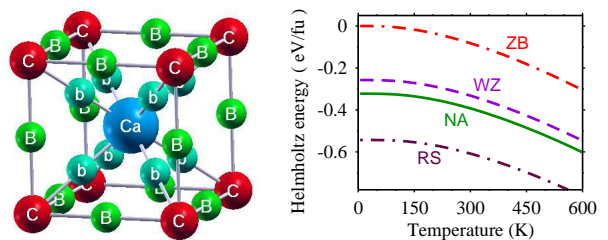


FIG. 9: (Color online) Left: Calculated topological bonds in B2-CaC, The green balls with letters b and B stand for the ionic Ca-C and covalent C-C bond points, respectively. Right: Helmholtz free energy of the ferromagnetic CaC structures as a function of temperature.

erties. The vibrational based thermodynamic properties of a system is studied by calculating the vibrational contribution to the Helmholtz free energy (F) as follows:

$$F(T) = E - k_B T \int d\omega D(\omega) \ln\left(\frac{e^{-\beta\hbar\omega/2}}{1 - e^{-\beta\hbar\omega}}\right)$$

where E is the total energy of the system, the integration is over the phonon frequencies, $D(\omega)$ is the phonon DOS, k_B is the Boltzmann constant, T is the kelvin temperature, and $\beta = 1/k_B T$. By inserting the calculated phonon DOS into the above equation, the Helmholtz free energy of CaC in its four ferromagnetic structures were calculated and presented in (Fig. 9). The results indicate absence of any temperature induced structural phase transition in the ferromagnetic structures of CaC.

Finally, we have used our first-principle phonon spectra to calculate various mechanical properties of the ferromagnetic structures of CaC (table V). The Debye temperature (T_D), which measures hardness of a solid, was calculated by using the speed of sound and density of atoms in the system.¹⁸ The elastic constants are calculated from the slopes of the acoustic phonon bands at the Γ point.¹⁹ The obtained elastic constants were used to calculate several mechanical parameters, listed in table V. The cubic and hexagonal bulk B and shear G moduli are calculated from the elastic constants,²⁰ and then the Young modulus (Y) is calculated by $Y = 9BG/(3B + G)$. In the cubic ZB and RS lattices, we observe that the phonon based bulk and Young moduli are close to the directly calculated values (table V). This consistency confirms reliability and accuracy of our phonon frequency calculations. In the hexagonal structures, two schemes proposed by Reuss and Voigt,²⁰ are applied for calculating the bulk and shear moduli from the elastic constants. In the NA structure we found that the Reuss scheme gives better bulk and Young moduli, compared with the directly calculated values, while in the hexagonal WZ structure, the Voigt scheme exhibits better performance. The B/G ratio, presented in table V, qualitatively determine the ductility of a material.²¹ Therefore, among the ferromagnetic structures of CaC, the most ductile and brittle systems are expected to be the ZB and RS structures, respectively. The mechanical parame-

TABLE V: Calculated mechanical properties of CaC in the RS, NA, WZ, and ZB structures, T_D (K): Debye temperature, C_{ij} (GPa): elastic constants, B_{ph} , Y_{ph} , and G_{ph} (GPa): bulk, Young, and shear moduli calculated from the elastic constants, B and Y (GPa): directly calculated bulk and Young moduli from the energy-volume and energy-lattice parameter curves, and σ : poison ratio.

Structure	T_D	C_{11}	C_{33}	C_{44}	C_{66}	C_{12}	C_{13}	B_{ph}	B	Y_{ph}	Y	G_{ph}	B/G	σ
RS	470	153		58		13		60	60	139	124	63	0.95	0.08
NA	466	131	196	55	72	-14	13	54	57	138	149	64	0.84	0.05
WZ	459	76	200	10	13	49	2	49	48	55	57	27	1.81	0.27
ZB	458	53		20		36		42	42	42	44	16	2.63	0.40

ter poison ratio, calculated by $\sigma = 1/2(1 - Y/3B)$, may be qualitatively used to compare structural stiffness of materials; more stiff materials have lower poison ratios. Hence the RS and NA structures of CaC are expected to be more stiff systems, compared with the WZ and ZB structures.

VI. CONCLUSIONS

In this paper we employed density functional-pseudopotential calculations to study structural, magnetic, and mechanical properties of the zinc-blende (ZB), wurtzite (WZ), rock-salt (RS), B2, NiAs (NA), and anti-NiAs (NA*) structures of CaC compound. Considering the transferred charge from cation to anion as well as the electron density at bond points, we found that the covalency of the system increases along the ZB-WZ-NA-RS-B2-NA* sequence, while the ionicity decreases. As a result of that, the NA* and B2 structures exhibit the lowest cohesive energies and nonmagnetic ground states while the ZB structure is the highest energy metastable system with the half-metallic property. Investigation of the enthalpy free energy of the systems along with the observed dynamical instabilities of the NA* and B2 structures showed that the ferromagnetic RS structure is the most stable system at the equilibrium conditions while

stabilization of the half-metallic ZB and WZ structures requires some negative hydrostatic pressures (lattice expansions). The dynamical instabilities of the nonmagnetic NA* and B2 structures were attributed to the observed tendency of the carbon atoms toward reconfiguration (possibly dimerization). The observed \mathbf{p} ferromagnetism in the ZB, RS, WZ, and NA structures of CaC was argued to be due to the strong ionic interaction between calcium and carbon which give rises to a sharp partially filled \mathbf{p} band on the carbon atom. The interatomic exchange stiffness of the ferromagnetic CaC structures were speculated to be higher than 20 meV. Because of the less influence of the crystal symmetries on the \mathbf{p} orbital, the magneto-structural coupling in the \mathbf{p} magnetic systems was argued to be weak. The application of the non-local exchange interaction via the screened HSE03 hybrid functional resulted in a perfect Fermi level spin polarization and half-metallic behavior for all ferromagnetic CaC structures.

VII. ACKNOWLEDGMENT

This work was jointly supported by the Vice Chancellor of Isfahan University of Technology (IUT) in research affairs, ICTP affiliated centre in IUT, and Centre of Excellence for Applied Nanotechnology.

* Electronic address: hashemifar@cc.iut.ac.ir

¹ O. Valnianska and P. Boguslawski, J. Phys.: Condens. Matter **22**, 073202 (2010).

² K. Kusakabe, M. Geshi, H. Tsukamoto, and N. Suzuki, J. Phys.: Condens. Matter **16**, S5639 (2004).

³ M. I. Katsnelson, V. Y. Irkhin, L. Chioncel, A. I. Lichtenstein, and R. A. de Groot, Rev. Mod. Phys. **80**, 315 (2008).

⁴ M. Sieberer, J. Redinger, S. Khmelevskiy, and P. Mohn, Phys. Rev. B **73**, 024404 (2006).

⁵ N. N. Greenwood and A. Earnshaw, *Chemistry of Elements* (Elsevier, 1997).

⁶ P. Giannozzi, S. Baroni, N. Bonini, M. Calandra, R. Car, C. Cavazzoni, D. Ceresoli, G. Chiarotti, M. Cococcioni, I. Dabo, et al., Journal of Physics: Condensed Matter **21**, 395502 (19pp) (2009), URL

<http://www.quantum-espresso.org>.

⁷ J. P. Perdew, S. Burke, and M. Ernzerhof, Phys. Rev. Lett. **77**, 3865 (1996).

⁸ We used the FHI norm-conserving pseudopotentials `ca.optgga2.fhi` and `c.optgga1.fhi` from <http://opium.sourceforge.net> and transformed them to the implemented pseudopotentials for the QUANTUM-ESPRESSO package.

⁹ H. J. Monkhorst and J. D. Pack, Phys. Rev. B. **13**, 5188 (1976).

¹⁰ M. Methfessel and A. T. Paxton, Phys. Rev. B **40**, 3616 (1989).

¹¹ S. Baroni, S. de Gironcoli, A. Dal Corso, and P. Giannozzi, Rev. Mod. Phys. **73**, 515 (2001).

¹² Topology of Electronic Charge Density (TECD) is a suite of Fortran programs, Developed by Dr. Stern with fund-

- ing from the Defense Advanced Research Project Agency. It calculates and analyzes the topology of a numerical charge density data file calculated with density functional techniques, such as Vienna Ab-Initio Simulation Package (VASP) and Amsterdam Density Functional (ADF). See <http://inside.mines.edu/meberhar/new1/MTG/software.shtml>.
- ¹³ F. Murnaghan, Proceedings of the national academy of sciences of the United States of America **30**, 244 (1944).
- ¹⁴ E. Şaşıoğlu, L. Sandratskii, P. Bruno, and I. Galanakis, Phys. Rev. B **72**, 184415 (2005).
- ¹⁵ G. Y. Gao, K. L. Yao, E. Şaşıoğlu, L. M. Sandratskii, Z. L. Liu, and J. L. Jiang, Phys. Rev. B **75**, 174442 (2007).
- ¹⁶ M. Grüning, A. Marini, and A. Rubio, J. Chem. Phys. **124**, 154108 (2006).
- ¹⁷ J. Heyd, G. E. Scuseria, and M. Ernzerhof, J. Chem. Phys. **118**, 8207 (2003).
- ¹⁸ $T_D = (\hbar v_s/k_B)(6\pi^2 N/V)^{1/3}$, v_s is the speed of sound calculated from the slop of the acoustic phonon band at the Γ point, N is the number of atoms in crystal, V is the crystal volume, and k_B is the Boltzmann constant [Ch, Kittel, *Introduction to solid state physics*, 7th Ed., (Wiley, 1996)].
- ¹⁹ S. Haussuhi, *Physical Properties of Crystal* (Wiley, 2007).
- ²⁰ Cubic lattices [Gene Simmons and Herbert Wang, *single Crystal Elastic Constants and Calculated Aggregate Properties*, (The MIT Press, 1971)]:
 $B = (C_{11} + 2C_{12})/3$ and $G = (3C_{44} + C_{11} - C_{12})/5$
 Non-cubic lattices - Voigt scheme [W. Voigt, *Lehrbuch der Kristallphysik* (1928), page 739]:
 $B = [(C_{11} + C_{12})C_{33} - 2C_{13}^2]/[C_{11} + C_{12} + 2C_{33} - 4C_{13}]$
 $G = 5/2[(C_{11} + C_{12})C_{33} - 2C_{12}^2]C_{55}C_{66}/[3BC_{55}C_{66} + [(C_{11} + C_{12})C_{33} - 2C_{13}^2]^2(C_{55} + C_{66})]$
 Non-cubic lattices - Reuss scheme [A. Reuss and Z. Angew. Math. Mech. **9**, 49 (1929)]:
 $B = (2C_{11} + 2C_{12} + 4C_{13} + C_{33})/9$
 $G = 1/30C_{11} + C_{12} + 2C_{33} - 4C_{13} + 12C_{44} + 12C_{66}$.
- ²¹ S. F. Pugh, Philos. Mag. **45**, 823 (1954).